2-Aminopyrimidine-silver(I) based organic semiconductors: Electronic structure and optical response

A. Riefer,* E. Rauls, and W. G. Schmidt
Lehrstuhl für Theoretische Physik, Universität Paderborn, 33095 Paderborn, Germany

J. Eberhard, I. Stoll, and J. Mattay
Organische Chemie I, Universität Bielefeld, 33615 Bielefeld, Germany

(Received 8 September 2011; revised manuscript received 30 January 2012; published 4 April 2012)

Calculations based on (occupation constrained) density functional theory using local as well as hybrid functionals to describe the electron-electron exchange and correlation are combined with many-body perturbation theory in order to determine and rationalize the electronic and optical excitation properties of 2-aminopyrimidine-silver(I) based organic semiconductors and their parent molecules. Large quasiparticle shifts and exciton binding energies of about 4 eV are found in the aminopyrimidine molecules. Both the quasiparticle blueshift and the excitonic redshift are reduced upon crystal formation. They cancel each other partially and thus allow for a meaningful description of the molecular and crystal optical response within the independent-particle approximation. We find a surprisingly strong influence of local-field effects as well as resonant-nonresonant coupling terms in the electron-hole Hamiltonian on the optical properties. The calculations reproduce well measured data and allow for identifying chemical trends with respect to the organic building blocks of the crystals.

DOI: 10.1103/PhysRevB.85.165202 PACS number(s): 71.20.Rv, 78.40.Me

I. INTRODUCTION

Organic semiconductors are important materials for various applications due to their low cost fabrication processes and the possibility to fine-tune desired functions by chemical modification of their building blocks. While the past years have seen a tremendous progress in the understanding of the excitation properties of inorganic semiconductors, fueled in part by the availability of advanced computational schemes for electronic structure and optical response calculations such as the GW approximation (GWA) for obtaining accurate electronic quasiparticle energies and the Bethe-Salpeter approach (BSE) to calculate electron-hole interaction effects,[1–6] far less is known about the electronic and optical properties of organic crystals. The electronic and optical properties of molecular crystals are fundamentally different from those of inorganic metals and semiconductors, due to weak intermolecular interactions of, e.g., van der Waals or hydrogen-bond type. The complicated interplay of intra- and intermolecular excitations renders the modeling and interpretation even of exceedingly simple molecular crystals such as solid water a methodological and computational challenge.[7–9] The modeling and understanding of electronic and optical excitation in crystals consisting of larger and more complex molecular constituents promises to be even more interesting.[10–15] Apart from the chemical properties of the single molecular constituents, the electronic and optical characteristics are largely emerging from the solid state assembly of the organic building blocks.

Recently, a novel class of organic electronic material has been synthesized by the self-assembly and silver(I) complex formation of 2-aminopyrimidines.[16] The compounds were structurally as well as optically characterized[17] and it was found that the solid state absorption differs remarkably from the parent compound 2-aminopyrimidine. The optical properties could be tuned by changing the silver counterion or by the reversible solvent extrusion and interchange. Furthermore, the electrical conductivity of the material was proven for a thin crystalline film.

Here we present *first-principles* calculations on the electronic and optical properties of 2-aminopyrimidine-silver(I) based organic semiconductors and their constituents in order to clarify the impact of many-body effects, intermolecular interactions, and chemical trends for this novel class of materials. The calculated optical response is compared with absorption measurements. In detail, we study 5-(pentafluorophenyl)pyrimidin-2-amine (FAP), 5-(4-methoxy-2,3,5,6-tetrafluorophenyl)pyrimidin-2-amine (OFAP), and 5-(4-(dimethylamino)-2,3,5,6-tetrafluorophenyl)pyrimidin-2-amine (NFAP) as well as their solid state assembly with the silver salts AgX with $X = CO_2CF_3$, NO_3, and SO_3CF_3. The three aminopyrimidine molecules (APM) are shown in Fig. 1. They consist of 22 (FAP), 26 (OFAP), and 30 (NFAP) atoms forming a 2-aminopyrimidine ring (atoms 1 to 8 in Fig. 1) and a (per)fluorinated phenylring ring (12 to 17) where the attached unit is either a fluorine atom F_1 (FAP), a methoxy group (OFAP), or an amino group (NFAP).

Depending on the involved silver salt, the crystalline solids are made of one-dimensional polymer strands (exemplarily shown in Fig. 2) with different lattice parameters and space groups (Table I). The assembly of APM with the salts $AgCO_2CF_3$ and $AgNO_3$ results in a unit cell containing a multiple of the molecular unit and the AgX pair. The crystallization with $AgSO_3CF_3$ results in unit cells where in addition to APM and AgX also solvent molecules (SOM) are contained. In case of FAP and $AgSO_3CF_3$, the solvent molecules are either ethanol (EtOH) or isopropanol (iPrOH). The number of AgX + APM or AgX + APM + SOM building blocks in one unit cell ranges from 2 to 8 which results altogether in 60–352 atoms. In order to clarify the influence of the silver salt on the excitation properties of crystalline

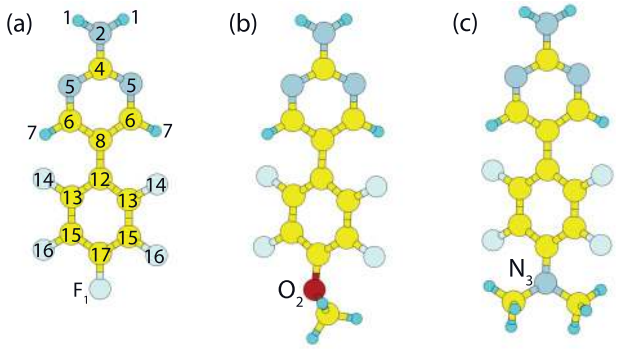

FIG. 1. (Color online) Schematic model of 5-(pentafluorophenyl)pyrimidin-2-amine (FAP), 5-(4-methoxy-2,3,5,6-tetrafluorophenyl)pyrimidin-2-amine (OFAP), and 5-[4-(dimethylamino)-2,3,5,6-tetrafluorophenyl]pyrimidin-2-amine (NFAP) (from left to right). Dark (red), light (yellow), gray, light gray, and small balls indicate O, C, N, F, and H atoms, respectively.

solids, we also investigate a crystal ($NFAP_s$, consisting of 480 atoms) which is bonded due to fluoroarene-stacking and hydrogen-bonding rather than via Ag complex formation; see Table I. Detailed structural information on the systems investigated can be found in Ref. 18.

II. METHODOLOGY

A. General

Ground-state and GWA calculations are performed using the Vienna *Ab-initio* Simulation Package (VASP) implementation[19] of the gradient-corrected[20] density functional theory (DFT-GGA). The electron-ion interaction is described by the projector augmented-wave method.[21,22] We expand the valence wave functions into plane waves up to an energy cutoff of 400 eV. DFT calculations for single molecules were performed using a $14 \times 15 \times 20$ Å^3 super cell and Γ point sampling for the Brillouin zone (BZ) integration. Within the unit cell, the molecules are positioned such that the lateral interactions have been minimized. Test calculations show that the eigenenergies are converged within a few hundredths an eV. For electronic self-energy calculation applying perturbation theory (G_0W_0) and Bethe-Salpeter type calculations (see below) for single molecules (see, e.g., Ref. 5) as well as for calculations of charged molecules the cell size was varied as described in Sec. III. In case of crystalline structures BZ integrations are performed using Γ centered meshes with the number of **k** points given in Table I. Thereby the calculations are based on the crystal lattice parameters determined experimentally. The internal degrees of freedom, however, were fully relaxed. A maximum shift of 0.37 Å compared to the initial coordinates taken from the x-ray structure determination was observed. Our DFT-GGA calculations result in bulk Ag band structures and optical spectra that agree with earlier calculations on the same level of theory; see, e.g., Refs. 23 and 24.

B. Electronic excitations

DFT calculations are known to often considerably underestimate electronic excitation energies.[4] Reliable quasiparticle gaps, exciton pair energies, and Stokes shifts for molecules and clusters, however, can be obtained from occupation constraint DFT (or ΔSCF) methods; cf. Refs. 8 and 25–28. Thereby the quasiparticle (QP) gap is obtained directly as the difference between the ionization energy and electron affinity,

$$E_g^{\mathrm{QP}} = E(N+1,\vec{R}) + E(N-1,\vec{R}) - 2E(N,\vec{R}), \qquad (1)$$

where $E(N,\vec{R})$, $E(N+1,\vec{R})$, and $E(N-1,\vec{R})$ represent the energy of a N, $N+1$, and $N-1$ electron system, respectively, with the equilibrium geometry $\vec{R}$ of the N electron system. The energy of the lowest excitonic excitation corresponding to the situation that one electron occupies the lowest unoccupied molecular orbital (LUMO) leaving a hole behind in the highest occupied molecular orbital (HOMO) is given by

$$E_{\mathrm{ex}} = E(e-h,\vec{R}) - E(N,\vec{R}), \qquad (2)$$

where $E(e-h,\vec{R})$ is the total energy of the system in the presence of the electron-hole pair with fixed geometry $\vec{R}$. Alternatively, as can be derived from Janak's theorem (see Ref. 25), the energy of the lowest optical excitation can be obtained from the difference of the eigenenergies of the half-occupied HOMO $\varepsilon_{H,0.5}$ and LUMO $\varepsilon_{L,0.5}$, respectively,

$$E_{\mathrm{ex}} \simeq E_{\mathrm{ex}}^{J} = \varepsilon_{L,0.5} - \varepsilon_{H,0.5}. \qquad (3)$$

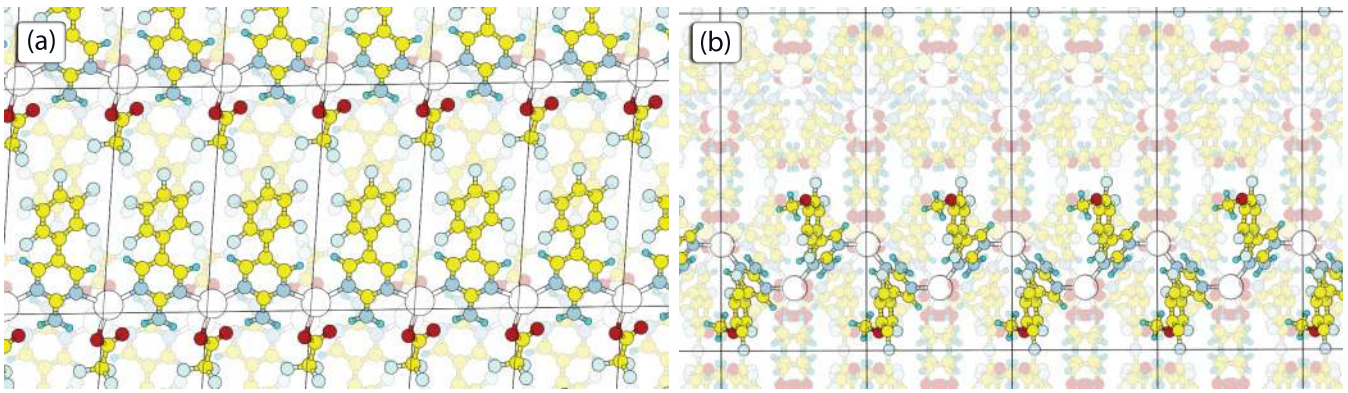

FIG. 2. (Color online) One-dimensional polymer strands in FAP + $AgCO_2CF_3$ (FAP_1, left) and OFAP + $AgSO_3CF_3$ + EtOH ($OFAP_{3a}$, right). Large (white) and large-light (large-yellow) balls indicate Ag and S atoms. Further colors are chosen in accordance with Fig. 1.

TABLE I. Crystalline solids derived from FAP, OFAP, and NFAP by silver complexation that have been studied in the present work. Given are information about solvent molecules (if applicable), crystal symmetry, the number of aminopyrimidine molecules N_m and atoms N_a per unit cell, and the **k**-point mesh used in the calculations for electronic and optical (geometrical) properties.

MOL	AgX + SOM	Abbreviation	Space group	N_m	N_a	**k**-point set
FAP	$AgCO_2CF_3$	FAP_1	$P-1$	2	60	$3\times3\times2$
	$AgNO_3$	FAP_2	$P21/c$	4	108	$2\times2\times2$
	$AgSO_3CF_3$ + EtOH	FAP_{3a}	$C2/c$	8	320	$1\times2\times2$
	$AgSO_3CF_3$ + iPrOH	FAP_{3b}	$P21/c$	4	172	$2\times2\times2$
OFAP	$AgCO_2CF_3$	$OFAP_1$	$Pbca$	8	272	$2\times2\times1$
	$AgNO_3$	$OFAP_2$	$P21/c$	4	124	$2\times2\times3$ ($1\times2\times2$)
	$AgSO_3CF_3$ + EtOH	$OFAP_{3a}$	$C2/c$	8	352	$1\times2\times2$
NFAP	–	$NFAP_s$	$Fddd$	16	480	$1\times1\times1$
	$AgCO_2CF_3$	$NFAP_1$	$C2/c$	8	304	$2\times4\times2$ ($1\times2\times1$)
	$AgSO_3CF_3$ + EtOH	$NFAP_{3a}$	$P21/c$	4	192	$2\times2\times1$

Relaxing the atomic coordinates to the geometry $\vec{R}^*$ for fixed occupation numbers yields the lowest emission energy,

$$E_{\rm em} = E(e-h,\vec{R}^*) - E(N,\vec{R}^*), \tag{4}$$

which can be used to calculate the Stokes shift,

$$\Delta_S = E_{\rm ex} - E_{\rm em}. \tag{5}$$

From calculations of the ground-state energy for different cell sizes one can conclude an error for the ΔSCF values of 0.1 eV. For the molecules, the obtained QP gaps $E_g^{\rm QP}$ are compared to the gap $E_g^{G_0W_0}$ that has been obtained from the G_0W_0 approximation of the electronic self-energy and is obtained by postprocessing the PW91 wave functions and eigenvalues. The implementation details are given in Ref. 29. Computational details are discussed in Sec. IV.

The excitation energies of extended structures such as crystalline solids cannot be obtained from ΔSCF calculations. In the present case, where the unit cells contain typically more than one hundred atoms, G_0W_0 calculations are also not feasible due to the high computational costs. Therefore, quasiparticle effects for the solid state are addressed in the present work by either using the hybrid functional HSE06[30–32] to calculate the electron exchange and correlation energy or by using a scissors operator, i.e., increasing the energies of the conduction bands by a constant amount.

C. Optical spectra

For semiconducting systems where the Bloch states have either the occupancy 0 for conduction bands, $n=c$, or 1 for valence bands, $n=v$, one obtains the dielectric tensor in independent-particle approximation[33–36] (IPA),

$$\epsilon_{ij}(\omega) = \delta_{ij} + \frac{4\pi e^2}{\Omega}\lim_{\mathbf{q}\to0}\frac{1}{q^2}\sum_{\mathbf{k}cv} 2\frac{1}{\varepsilon_c(\mathbf{k})-\varepsilon_v(\mathbf{k})-(\hbar\omega+i\eta)} \times \langle u_{c\mathbf{k}+\mathbf{q}_i}|u_{v\mathbf{k}}\rangle\langle u_{c\mathbf{k}+\mathbf{q}_j}|u_{v\mathbf{k}}\rangle^*, \tag{6}$$

where the sum $\sum_{\mathbf{k}}$ is to be taken over the first BZ, $\mathbf{q}_i$ is the reciprocal vector in the Cartesian direction i, $u_{n\mathbf{k}}$ are the periodic parts of the Bloch wave functions, $\varepsilon_n(\mathbf{k})$ the respective eigenenergies, Ω is the crystal volume, and η is the broadening.

In order to allow for comparison with the experimental data we average over the three Cartesian directions to

$$\epsilon(\hbar\omega) = \frac{1}{3}\sum_{i=x,y,z}\epsilon_{ii}(\hbar\omega). \tag{7}$$

The dielectric function within the IPA or by solving the BSE is based on the electronic structure as obtained from either the PW91/HSE06 calculations (partially with scissors shifted eigenvalues) or from the GWA.

Solving the Bethe-Salpeter equation includes the electron-hole attraction and local-field effects in the dielectric function. For practical calculations, the BSE is transformed into a two-particle Schrödinger equation.

Neglecting dynamical screening and umklapp processes, the resonant part of the exciton Hamiltonian [Tamm-Dancoff approximation (TDA); cf. Ref. 37] for direct transitions and spin-singlets can be calculated in reciprocal space according to

$$\hat{H}^{\rm res}_{vc\mathbf{k},v'c'\mathbf{k}'} = \left[\varepsilon_c^{\rm QP}(\mathbf{k})-\varepsilon_v^{\rm QP}(\mathbf{k})\right]\delta_{vv'}\delta_{cc'}\delta_{\mathbf{k}\mathbf{k}'} + \frac{4\pi}{\Omega}\sum_{\mathbf{G},\mathbf{G}'}\left\{2\frac{\delta_{\mathbf{G}\mathbf{G}'}(1-\delta_{\mathbf{G}\mathbf{0}})}{|\mathbf{G}|^2}B^{\mathbf{k}\mathbf{k}}_{cv}(\mathbf{G})B^{\mathbf{k}'\mathbf{k}'*}_{c'v'}(\mathbf{G}) - \frac{\epsilon^{-1}(\mathbf{k}-\mathbf{k}'+\mathbf{G},\mathbf{k}-\mathbf{k}'+\mathbf{G}',0)}{|\mathbf{k}-\mathbf{k}'+\mathbf{G}|^2} \times B^{\mathbf{k}\mathbf{k}'}_{cc'}(\mathbf{G})B^{\mathbf{k}\mathbf{k}'*}_{vv'}(\mathbf{G}')\right\}, \tag{8}$$

where the Bloch integral

$$B^{\mathbf{k}\mathbf{k}'}_{nn'}(\mathbf{G}) = \frac{1}{\Omega}\int d\mathbf{r}\, u^*_{n\mathbf{k}}(\mathbf{r})e^{i\mathbf{G}\mathbf{r}}u_{n'\mathbf{k}'}(\mathbf{r}) \tag{9}$$

over the periodic parts u of the Bloch wave functions has been introduced. In the actual calculations we replace the inverse dielectric matrix ϵ^{-1} by a diagonal model dielectric function suggested by Bechstedt *et al.*[38] It depends on the static dielectric constant ϵ_∞ and reduces the computational effort substantially. In the case of inorganic semiconductors,[39–41] molecular crystals,[7,8] and even surfaces,[42] the application of this model dielectric function leads to rather accurate results. This is related to the fact that the model dielectric function

depends on the local charge density and therefore carries some information about the local screening. For FAP_1 we applied the value $\epsilon_\infty = 2.51$ taken from IPA calculations. In the case of molecule calculations, the correct choice of ϵ_∞ is difficult. The authors of Ref. 15 defined an effective volume Ω_{eff} where the screening takes place in order to address this problem in their optical response calculation of poly-para-phenylenevinylene. In our work we use for molecular calculations $\epsilon_\infty = 1$, which marks the lower limit for the screening interaction. If one assumes $\Omega_{\text{eff}} = 18^3$ Å^3, the IPA calculations for FAP result in $\epsilon_\infty = 1.05$, which leads to a blueshift of the excitonic eigenvalues by about 0.3 eV. Calculations for further values of ϵ_∞ indicate a nearly linear dependence of the exciton binding energies on the screening, as may be expected.

The dimension of the exciton Hamiltonian [Eq. (8)] is determined by the size of the energy window for conduction and valence states. Here we include the states the Kohn-Sham eigenvalues of which satisfy $\varepsilon_c(\mathbf{k}) - \varepsilon_v(\mathbf{k}) < 14$ eV (16 eV) in the case of FAP_1 and PW91 (HSE06). The molecular spectra are calculated including either all states satisfying $\varepsilon_c(\mathbf{k}) - \varepsilon_v(\mathbf{k}) < 6$ eV (DFT) or the lowest 96 states (GWA). For the actual calculation of the spectra we use the time-evolution algorithm proposed by one of the present authors.[42]

Recent results[11,12,43] question the validity of the Tamm-Dancoff approximation for molecular systems. Therefore, in addition to BSE-TDA, also calculations with the full exciton Hamiltonian were performed (BSE).

For the comparison with measured optical spectra we use real and imaginary parts of the dielectric function, $\epsilon'(\hbar\omega)$ and $\epsilon''(\hbar\omega)$, respectively to obtain the attenuation coefficient α using the approximation

$$\alpha(\hbar\omega) \propto \hbar\omega\sqrt{[\sqrt{\epsilon'(\hbar\omega)^2 + \epsilon''(\hbar\omega)^2} - \epsilon'(\hbar\omega)]}. \qquad (10)$$

The calculated data are compared with optical absorption measurements on powder samples.

III. FAP, OFAP, AND NFAP MOLECULES

A. Geometry

The structural relaxation of FAP, OFAP and NFAP in gas phase shows that the geometry of the aminopyrimidine and pentafluorophenyl rings does barely change upon attachment of either a fluorine atom (FAP), a methoxy group (OFAP), or an amino group (NFAP). The comparison of our calculated data with x-ray data of two polymorphic crystals of the hydrogen analog 5-phenyl-pyrimidin-2-ylamine (HAP) and a HAP-hexafluorobenzene cocrystal[16] as well as the recently crystallized NFAP ligand itself shows only small differences in bond length and angles. Only for the hydrogen bonds we observe deviations of up to 0.10–0.16 Å between measured and calculated data. The geometries calculated here also closely agree with Møller Plesset perturbation theory (MP2) results for AMP[44]: The bond lengths deviate by less than 0.02 Å and the largest deviation of bond angles amounts to 3°.

B. Electronic excitations

Starting from the relaxed structures we calculated the quantities defined in Eqs. (1)–(5). The results for FAP, OFAP, and NFAP are compiled in Table II. We find that the difference of the HOMO and LUMO eigenenergies, $E_g^{\text{PW91}} = \varepsilon_L - \varepsilon_H$, is largest for FAP and decreases by going from OFAP to NFAP (see also Fig. 4 for the electronic levels), i.e., with increasing electron-donating properties. In HSE06 the ordering between FAP and OFAP is reverse compared to the GGA calculation. However, the gaps are very close. The trend observed with GGA holds also for the G_0W_0 gaps $E_g^{G_0W_0}$ and the ΔSCF gaps E_g^{QP}. The calculation of a QP ΔSCF gap requires the determination of the total energies $E(N+1,\vec{R})$ and $E(N-1,\vec{R})$ of charged molecules. Due to the interactions with the periodic images the dependence of the latter and thus the gap E_g^{QP} on the cell size is not negligible. In order to correct the calculated excitation energies, the gaps were determined for a cubic cell with varying size $L = 18, \ldots, 30$ Å. As shown in Fig. 3, the gap values depend linearly on $1/L$. Extrapolation to $L \to \infty$ leads to the gaps cited in Table II.

TABLE II. Electronic key quantities for FAP, OFAP, and NFAP (in eV).

	FAP	OFAP	NFAP
E_g^{PW91}	3.46	3.35	3.00
E_g^{HSE06}	4.53	4.55	4.21
$E_g^{G_0W_0}$	$\lesssim$7.7	$\lesssim$7.4	$\lesssim$7.1
E_g^{QP}	7.36	7.06	6.47
E_{ex}	3.51	3.46	3.21
E_{ex}^J	3.50	3.46	3.22
E_{em}	2.08	1.97	1.98
Δ_S	1.43	1.49	1.23

A dependence on the unit cell size is also noted for the calculated G_0W_0 gaps; see Fig. 3. To some extent, this is to be expected due to the periodic repetition of the molecules; see, e.g., Ref. 45. The restriction of the calculations with respect to further parameters due to numerical limitations, however, is even more important in the present case. The self-energy calculations for cubic cells with the size $L = 18$–20 Å (22–24 Å) were performed with a maximum cutoff for the response function of 60 eV (40 eV), 90 frequency points,

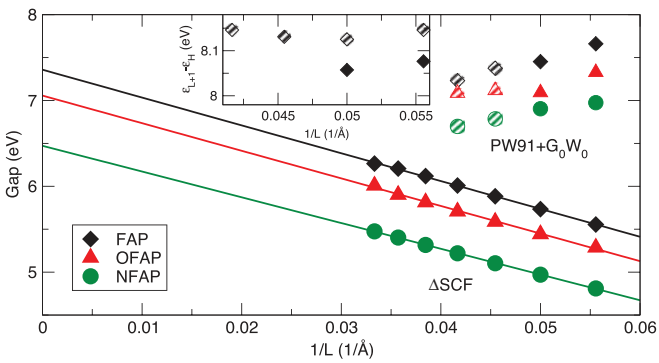

FIG. 3. (Color online) Dependence of the calculated quasiparticle gaps E_g^{QP} and G_0W_0 gaps $E_g^{G_0W_0}$ on the cell size L. The filled/striped symbols for G_0W_0 values denote calculations with a cutoff for the response function of 60/40 eV (see text). The inset shows the respective values for the energy difference between the LUMO + 1 and HOMO.

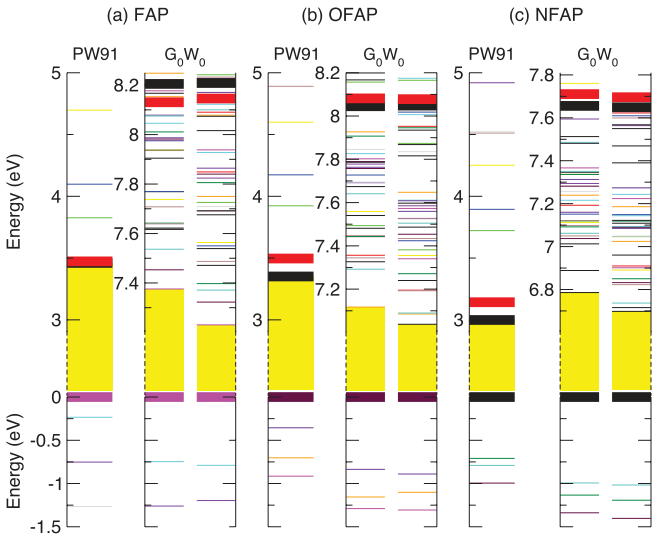

FIG. 4. (Color online) Energies of molecular orbitals as obtained from DFT (PW91) and G_0W_0 calculations for cubic cells with $L =$ 22 Å (left) and $L = 24$ Å (right). The influence of the self-energy corrections and cell size on the energy order of the states is indicated by different colors. Thick bars refer to the orbitals that correspond to HOMO, LUMO, and LUMO + 1 in the PW91 calculations. The fundamental gap is indicated. Note the different energy region for the empty states.

and a cutoff of 15–16 eV for the sum over empty states (including up to 1056 bands). Our results, as well as the comparison with numerics in similar work,[46] show that the self-energy calculations are not fully converged with respect to these parameters. The problem originates from the fact that the necessary usage of large unit cells for the gas-phase molecule calculations results in a large number of reciprocal lattice vectors that exceed the computer memory presently available to us. The dependence of the G_0W_0 on the numerics is obvious from the inset in Fig. 3, where the energy difference between the FAP HOMO and LUMO + 1 states is shown, but also from Fig. 4, where the energetic ordering of the electronic states is visualized. Obviously, the order changes upon inclusion of electronic self-energies calculated with the G_0W_0 approximation, but is itself not yet converged, at least for the unoccupied states. Nevertheless, as will be shown below, the reordering due to state-dependent self-energy corrections calculated in G_0W_0 improves the agreement between the measured and calculated optical absorption. The present data suggest that the band gaps calculated within the GWA decrease with increasing cell size for the molecules studied here. The numbers given in Table II should thus be considered as approximate upper limits. We find that the values are by about 0.5 eV larger than the respective energy gaps determined from the ΔSCF calculations. The fundamental gaps calculated with the HSE06 scheme, on the other hand, are between the PW91 and the quasiparticle gaps.

Interestingly, the quasiparticle shifts are nearly canceled by electron-hole attraction effects: the lowest electron-hole excitation energies E_{ex} are remarkably close to the difference of the HOMO and LUMO single-particle eigenenergies obtained from DFT. This near cancellation of many-body effects due to the electron-electron and the electron-hole interaction suggests that optical excitation spectra calculated in the independent-particle approximation may be a reasonable description at least for the low-energy excitations.

The calculation of the electron-hole excitation energies is computationally robust: the approaches according to Eq. (2) and Eq. (3) result in energies that agree within 0.01 eV. The lowest-energy excitations calculated for structural relaxation differ appreciable from the respective vertical excitation energies. We calculate Stokes shifts between 1.2 and 1.5 eV for the three molecules. Thereby, the energetic ordering changes between absorption and emission. While NFAP is predicted to have the lowest vertical excitation energy, its deexcitation occurs at slightly larger energies than OFAP.

Our calculated values are in reasonable agreement with the experimental data available. For FAP dissolved in ethanol Stoll *et al.*[17] measured a Stokes shift of 1.28 eV. Given that the optical response of the molecules will be influenced by the solvent, these data confirm the validity of the present calculations.

C. Optical excitations

From the eigenfunctions and eigenvectors obtained in DFT one can directly calculate the dielectric function in independent-particle approximation. Figure 5 shows the resulting spectra for FAP, OFAP, and NFAP. Obviously, in all three cases the onset of the optical absorption is larger than $E_g^{DFT} = \varepsilon_L - \varepsilon_H$ due to the small transition probability between HOMO and LUMO. There are more similarities in the spectra. In particular, FAP and OFAP agree largely concerning the positions and line shapes of the main peaks I–IV (see Fig. 5). Since the dielectric function in independent-particle approximation is composed of independent transitions between occupied and empty electronic states, it is straightforward to interpret. In case of the FAP dielectric function, for example, it turns out that the HOMO–LUMO + 1 transition is responsible for 86% of the intensity of the first absorption peak.

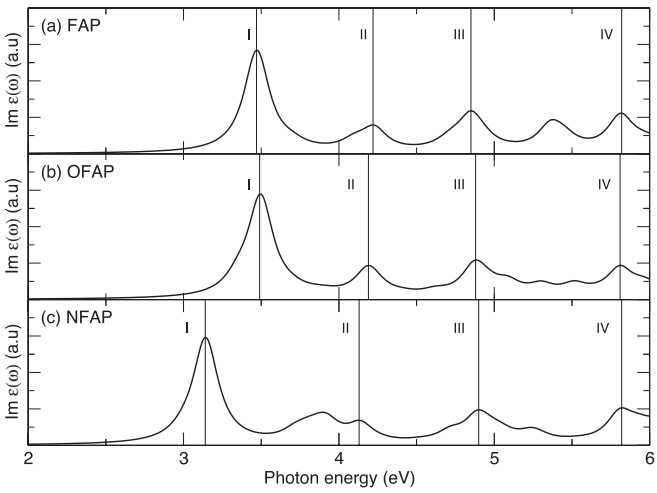

FIG. 5. Imaginary part of the dielectric function calculated in independent-particle approximation for FAP, OFAP, and NFAP. A broadening of $\eta = 0.10$ eV has been used.

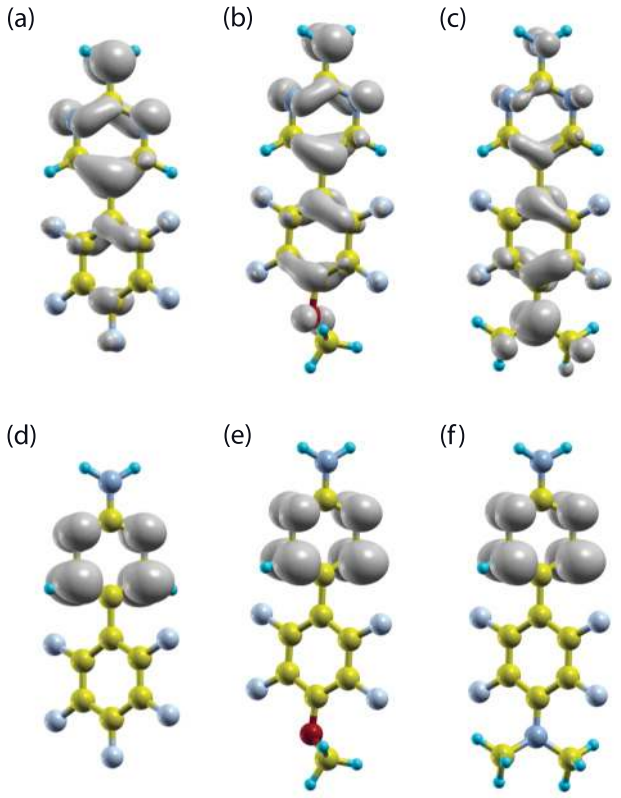

FIG. 6. (Color online) Orbital character of the states HOMO (a)–(c) and LUMO (d)–(f) for FAP, OFAP, and NFAP.

For further systematic analysis of the spectra, we characterize the electronic wave functions of state λ according to their localization. To this end we calculate the projection of the corresponding state onto spherical harmonics Y_{lm}^{n} centered at specific atoms n,

$$\alpha_{n\lambda} = \sum_{lm} \left|\langle \phi_\lambda | Y_{lm}^{n} \rangle\right|^2, \tag{11}$$

and sum over all atoms n belonging to either the aminopyrimidine and pentafluorophenyl rings (M) or the attached fluorine atom, methoxy, or amino group (R),

$$\alpha_{M/R\lambda} = \sum_{n \in M/R} \alpha_{n\lambda}. \tag{12}$$

Evaluating the quantities $\alpha_{M\lambda}$ and $\alpha_{R\lambda}$ allows for a quantitative understanding of the origin of the major peaks in the optical spectra of FAP, OFAP, and NFAP. In particular, we find that transitions between HOMO and LUMO + 1 are essentially causing the first absorption peak for all three molecules. The data show furthermore that the optical absorption occurs largely due to states localized at the aminopyrimidine and pentafluorophenyl rings. This explains why the optical response of the three molecules shown in Fig. 5 is rather similar. A notable exception is the first absorption peak of NFAP. In this case the HOMO is strongly influenced by amino-group localized states (cf. Fig. 6 and Table III). Contributions of the attached fluorine atom or the methoxy group are—to a much smaller extent—also present in the first absorption peak of FAP or OFAP (cf. Fig. 6 and Table III).

TABLE III. Calculated relative contribution of the electronic states HOMO and LUMO + 1 to the first optical absorption peak for IPA (Fig. 5) and to the state $|I\rangle$ for BSE/BSE-TDA based on either the scissors shifted PW91 or G_0W_0 electronic structure (cf. Fig. 7) of FAP, OFAP, and NFAP. Also given are the quantities $\alpha_{M/R\lambda}$ for the respective HOMO and LUMO + 1.

	FAP	OFAP	NFAP
IPA			
Energy (eV)	3.47	3.49	3.14
Intensity (%)	86	94	97
$\alpha_{M(\mathrm{HOMO})}$	0.58	0.54	0.33
$\alpha_{R(\mathrm{HOMO})}$	0.01	0.06	0.28
$\alpha_{M(\mathrm{LUMO+1})}$	0.53	0.52	0.50
$\alpha_{R(\mathrm{LUMO+1})}$	0.02	0.03	0.04
BSE-TDA (PW91 + Δ)			
Energy (eV)	3.70	3.51	3.02
A_I(HOMO)	57	57	71
A_I(LUMO + 1)	69	57	67
BSE (PW91 + Δ)			
Energy (eV)	3.65	3.46	2.97
A_I(HOMO)	65	59	77
A_I(LUMO + 1)	75	62	74
BSE(G_0W_0)			
Energy (eV)	4.48	4.36	4.05
A_I(HOMO)	65	65	76
A_I(LUMO + 1)	75	75	71

In Fig. 7 the molecular dielectric functions calculated by taking many-body effects into account are shown. The calculations have been performed using the full excitonic Hamiltonian as well as applying the TDA. The empty electronic levels were

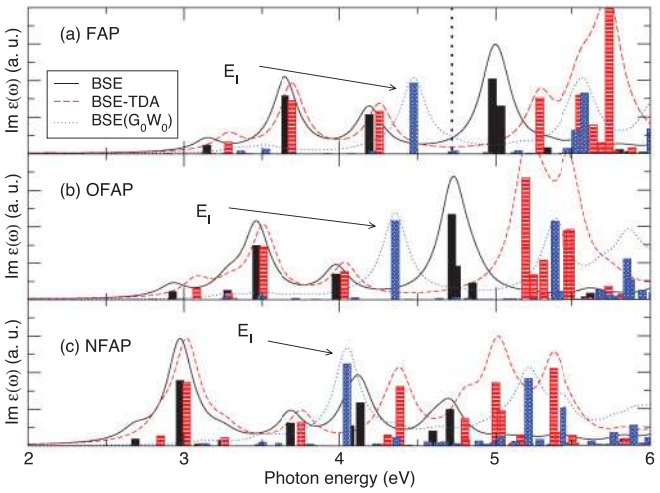

FIG. 7. (Color online) Imaginary part of the dielectric function calculated by solving the BSE based on G_0W_0 calculations or by applying a respective scissors shift to reproduce the ΔSCF gaps or for FAP (a), OFAP (b), and NFAP (c). A broadening of $\eta = 0.10$ eV has been used. The solid (dashed)/dotted curve and bars gives the spectra and oscillator strengths versus the eigenvalues calculated within BSE (BSE-TDA) on the basis of the scissors shifted PW91/G_0W_0 electronic structure. The eigenvalues contributing to the first peak are labeled. See Ref. 39 for details. The strongest absorption maximum of FAP dissolved in ethanol[17] is shown by a dotted line.

either shifted such that the respective molecular ΔSCF gaps are reproduced or the G_0W_0 electronic structure was used as input. The red-shift of the first peak in the NFAP spectra compared to FAP and OFAP as observed in IPA occurs also on the BSE level of theory. It is even enhanced by the smaller respective value of the ΔSCF gap. In general the positions of the first optical absorption maxima calculated within the BSE agree within one eV with the IPA calculation, which is indicative for some cancellation of quasiparticle and excitonic shifts as already concluded from the values in Table II.

Similar to the IPA spectra discussed above we perform a systematic analysis of the states contributing to the respective absorption peaks by evaluating the quantities,[39,47]

$$A_\Lambda(c) = \sum_v |A_\Lambda(cv)|^2 \quad \text{and} \quad \mathrm{A}_\Lambda(\mathrm{v}) = \sum_c |\mathrm{A}_\Lambda(\mathrm{cv})|^2, \tag{13}$$

where $A_\Lambda(cv)$ are the eigenvectors corresponding to the respective eigenvalues $E_\Lambda > 0$ of the electron-hole Hamiltonian; see also Fig. 7. The quantities (13) for the states $|I\rangle$ carrying the largest oscillator strengths have been calculated. It turns out that—as already found on the IPA level of theory—HOMO and LUMO + 1 are the states that mostly contribute to the first adsorption peak; see Table III.

Comparing the spectra obtained from the full Hamiltonian and in TDA one finds distinct differences: (i) a redshift of the eigenvalues going from TDA to the full Hamiltonian as observed in Refs. 11 and 12 and (ii) strong modifications of the line shape for energies above 4.5 eV (FAP, OFAP) or 4.0 eV (NFAP); see also discussion in Sec. IV. While the Tamm-Dancoff approximation clearly affects the calculated optical absorption, in particular for excitations beyond the lowest absorption peak, we find the influence of the electronic structure that is used as input for the BSE calculations to be even more important. The optical spectrum based on the G_0W_0 electronic structure differs appreciably from the one based on scissors-shifted PW91 eigenvalues. This is due to the state-dependent self-energy corrections leading to an energetic reordering of the eigenvalue spectrum that results in a significant blueshift of the optical absorption data.

The measured position of the optical absorption peak of FAP dissolved in ethanol[17] in the energy window 2.3–5.7 eV is at 4.72 eV (vertical line in Fig. 7). Clearly, the BSE spectrum based on the G_0W_0 electronic structure agrees best with this value. It yields an optical absorption peak at 4.48 eV. From Table II it is clear that the error bar of the calculated excitation energies is of the order of several tenths of an eV. Moreover, as discussed in Sec. II C, our choice for the static dielectric constant used in the molecule calculations is bound to result in excitation energies that approach the real values from below. An additional uncertainty in the experiment-theory comparison is related to the fact that the solvent molecules are not included in the present gas-phase calculations. Therefore, the deviation between measured and calculated data of less than 0.3 eV is not surprising.

Comparing the computational results for the electronic states of FAP, OFAP, and NFAP summarized in Fig. 4 and the optical response from Figs. 6 and 7 one finds that the former are far more sensitive to the attachment of functional groups than the latter. Since the optical absorption essentially takes place at the aminopyrimidine and pentafluorophenyl rings, modifications in the molecular wave functions due to methoxy or amino group are only partially reflected in the optical data.

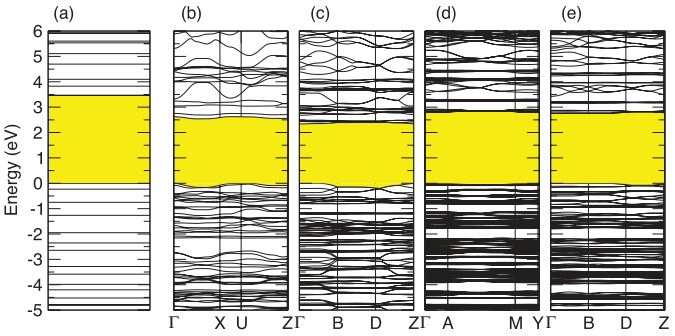

FIG. 8. (Color online) Comparison of the FAP molecular levels (a) calculated within DFT-GGA with the electronic band structure of FAP_1 (b), FAP_2 (c), FAP_{3a} (d), and FAP_{3b} (e). The fundamental gap is indicated.

IV. MOLECULAR CRYSTALS

A. Independent-particle calculations

The structural relaxation based on input data from the x-ray analysis is the starting point of the present calculations on the molecular crystals. Altogether we observe only small modifications of the geometrical parameters determined experimentally (see Ref. 18). The largest bond length deviation is 0.02 Å, while the bond angles agree within 3°.

Due to the condensation of the molecules to crystals, the discrete molecular energy levels calculated on the DFT level of theory broaden into energy bands as shown in Fig. 8 for the case of FAP derived compounds. The electronic band gap of the organic semiconductors is smaller than the difference of the HOMO and LUMO energies of the parent aminopyrimidine molecules. This is not only due to the broadening of the energy levels, but is also related to the newly arising Ag-N bonds. This is illustrated in Fig. 9, where the total as well as Ag projected density of electronic states (DOS) of FAP derived compounds is shown. Obviously, the electronic states close to the valence band maximum (VBM) have strong silver-related

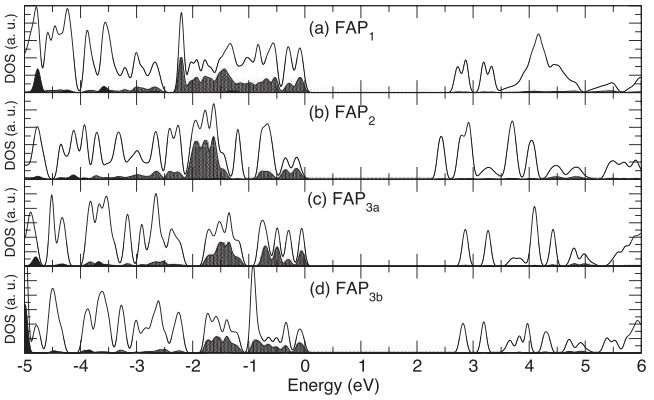

FIG. 9. Density of states (DOS, white area) calculated within DFT-GGA for FAP derived molecular crystals. Ag/F_1 (see Fig. 1) related contributions are indicated with dotted/black areas.

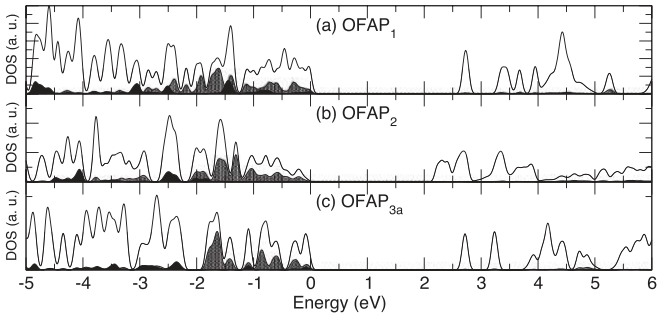

FIG. 10. Data as in Fig. 9, but for OFAP derived crystals. Methoxy group related contributions are indicated with black areas.

contributions. Similar findings are obtained for OFAP and NFAP derived compounds, as shown in Figs. 10 and 11, respectively.

In Figs. 12, 13, and 14 we compare the dielectric function calculated in independent-particle approximation for FAP, OFAP, and NFAP derived crystals with the corresponding calculations for the molecular species. In all three cases the molecular signatures are clearly visible in the spectra calculated for the organic semiconductor. This holds in particular for FAP derived systems, where the first molecular absorption peak constitutes the main absorption feature of the solids and does barely shift in energy. The spectrum calculated for NFAP$_s$ (not Ag-complex bonded) in comparison to NFAP$_1$ and NFAP$_{3a}$ in Fig. 14 indicates only a small influence of Ag-related states to the crystal optical response. Similarly, the influence of the solvent molecules is limited. The comparison between molecular and crystal spectra shows two main differences: (i) the semiconductor absorption features are broadened with respect to the molecular peaks due to the energy dispersion of the molecular states upon condensation, and (ii) optical absorption occurs also for photon energies below the onset of the molecular absorption due to optical transition involving silver related states. The overlap $\alpha_{\mathrm{Ag}\lambda}$ between spherical harmonics centered at silver atoms and wave functions of contributing valence states to transitions below the molecular gap can be up to 0.5 [see Eqs. (11) and (12)]. These observations hold also for OFAP and NFAP. In the case of NFAP, however, the optical response of the crystalline structures deviates more strongly from the respective molecular spectrum than observed for FAP and OFAP. In particular, the first absorption peak is redshifted. This is related to amino-group related optical transitions where the participating filled states (cf. black areas in Fig. 11) are close to the valence-band maximum.

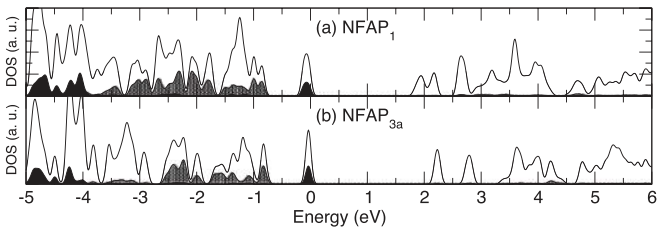

FIG. 11. Data as in Fig. 9, but for NFAP derived crystals. Amino group related contributions are indicated with black areas.

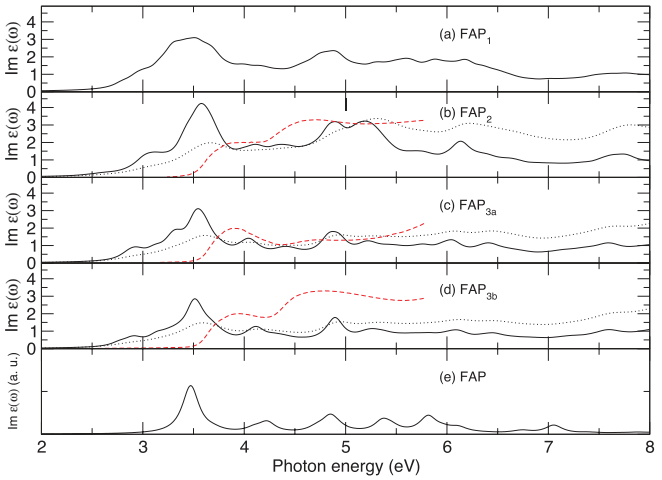

FIG. 12. (Color online) Imaginary part of the dielectric function based on the independent-particle approximation (IPA) for FAP derived molecular crystals in comparison with the corresponding calculation for FAP. A broadening of $\eta = 0.10$ eV has been used. Also shown is the experimental absorption spectra $i_a(\omega)$ (dashed line, in a.u.) and the calculated attenuation coefficient using Eq. (10) (dotted line, in a.u.).

B. Influence of many-body effects

Optical spectra calculated in the independent-particle approximation are well suited to identify and rationalize chemical trends[6] but their direct comparison with experimental results is complicated due to the influence of many-body effects in the electronic structure and in the optical spectra. To account for the former we calculated the HSE06 electronic structure for FAP$_1$. The calculated indirect/direct HSE06 band gap of 3.86/3.91 eV is in much better agreement with the experimental value of 3.50 eV[17] concluded from excitation spectra measurements than the corresponding HSE06 results for the gas-phase molecule. The indirect HSE06 gap exceeds the PW91 gap by 1.21 eV.

To study the influence of electron-electron correlation and electron-hole attraction as well as local-field effects on the absorption, we performed calculations for FAP$_1$; see Fig. 15. The dielectric function was calculated starting from the IPA

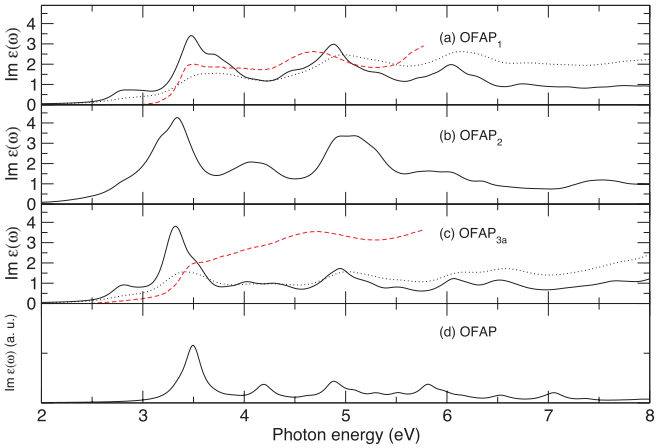

FIG. 13. (Color online) Data as in Fig. 12, but for OFAP derived crystals.

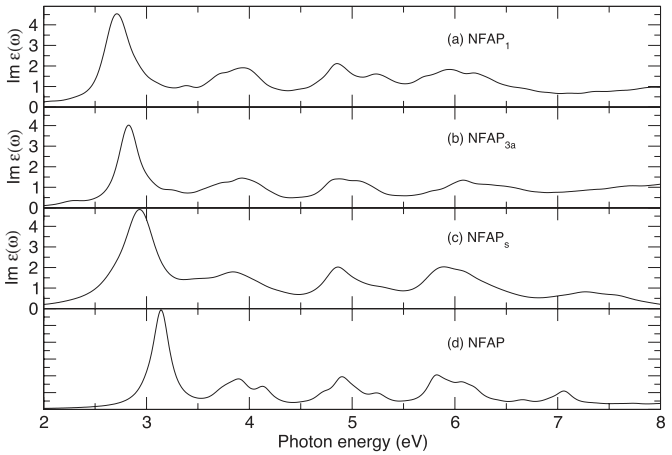

FIG. 14. Data as in Fig. 12, but for NFAP derived crystals.

based on the PW91 wave functions, including local-field effects, electron-hole interaction (BSE-TDA), and resonant-nonresonant coupling (BSE). One can observe the following features: (i) a remarkable blueshift of the order of 1 eV due to local-field effects also observed in Ref. 43, (ii) electron-hole attraction effect of the order of about 2 eV, and (iii) noticeable modifications of the line shape and to some extent also of the peak positions due to the resonant-nonresonant coupling terms in the excitonic Hamiltonian. As shown in Figs. 15(d) and 15(e), different components of the dielectric tensor are affected differently by the many-body effects.

While the strong effect of the electron-hole attraction on the optical spectra is known for many (also inorganic) semiconductors, the noticeable influence of local-field and resonant-nonresonant coupling effects seems to be peculiar to molecular systems.[11,12,43] To rationalize this effect we calculated the ratio β between the maximum off-diagonal element and the

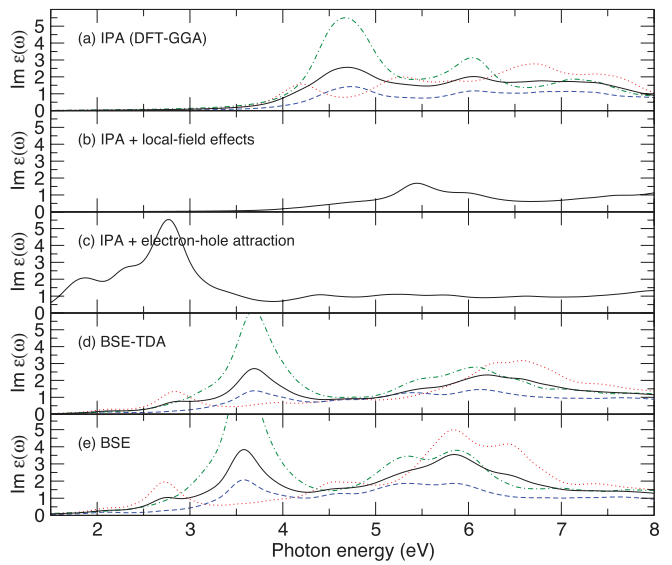

FIG. 15. (Color online) Comparison of the spectra for FAP_1 in different approximations. The spectra were calculated on top of the PW91-band structure and wave functions. A broadening of 0.2 eV and a scissors shift of 1.21 eV are applied. Also shown is $\epsilon_{xx}(\omega)$, $\epsilon_{yy}(\omega)$, and $\epsilon_{zz}(\omega)$ (dashed, dotted, and dash-dotted line).

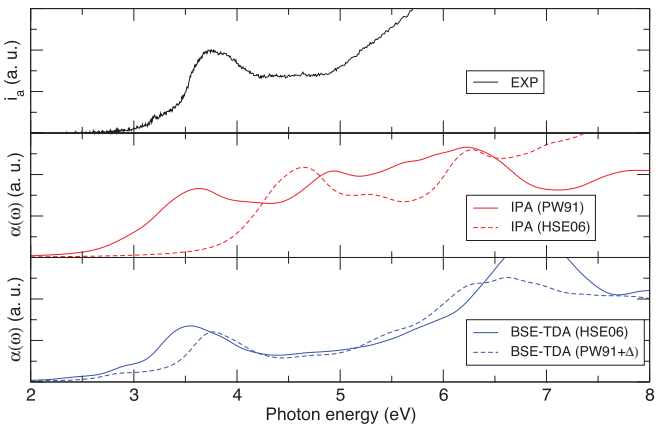

FIG. 16. (Color online) Optical spectra of FAP_1 calculated (see text) within the independent-particle approximation and from the Bethe-Salpeter equation in TDA (BSE-TDA) are compared with measured data from Ref. 17. Note that the attenuation coefficient [Eq. (10)] rather than the dielectric function is shown in order to facilitate the comparison with experiment.

minimum diagonal element of the electron-hole Hamiltonian. In the case of Si, for example, the off-diagonal elements are far smaller than the diagonal elements and therefore the TDA is valid.[2] In fact, β is of the order of 1 and 10^{-1} for FAP and FAP_1, respectively, whereas it amounts to $10^{-2}-10^{-3}$ for Si.[48,49] In order to better understand the reason for the failure of the TDA we further analyzed the exciton Hamiltonian in the case of FAP. It is found that although the average value of the off-diagonal elements of the BSE Hamiltonian is about $\sim 6 \times 10^{-2}$ eV—that are one to two magnitudes lower than the diagonal elements—there exists large off-diagonal matrix elements of the magnitude of 1–2 eV, partially from the diagonal of the nonresonant block, contributing to the resonant-nonresonant coupling. The largest of them are related to high energy transitions at $\varepsilon_c - \varepsilon_v + \Delta_{\mathrm{FAP}} \sim 9$–10 eV, where Δ_{FAP} is the scissors operator shift for FAP (see Sec. III C), with $(v,c) =$ (HOMO-5,LUMO), (HOMO-2,LUMO$+3$/LUMO$+1$), or (HOMO-3,LUMO$+3$). These transitions are characterized by a large spatial overlap of the corresponding wave functions. The fact that they occur at relatively large energies corresponds to our finding that the TDA becomes worse for larger excitation energies.

C. Comparison with experiment

How well do the calculations based on the independent-particle approximation describe the experiment? The calculated attenuation coefficient for FAP_1-FAP_{3b}, $OFAP_1$, and $OFAP_{3a}$ are compared with experimental data[17] in Figs. 12, 13, and 16. The energetic position of the absorption onset and especially in the case of FAP_2-FAP_{3b} and $OFAP_{3a}$ the line shape deviates somewhat from the IPA calculations. In Fig. 16 we compare the measured attenuation coefficient for FAP_1 with IPA and BSE-TDA calculations based on the PW91 or HSE06 electronic structure. The comparison with the experimental data shows that the results from the BSE-TDA calculations on top of the HSE06 electronic structure agree nicely with the measurements.[17] However, one has to state that numerically simpler calculations based on PW91 wave

functions and using a scissors shift $\Delta = 1.21$ eV (taken from the energy difference between the PW91 and HSE06 gap) to correct the band structure yield a similar degree of agreement with experiment. Obviously, the influence of the electronic structure used as input for the Bethe-Salpeter equation is not as pronounced for the molecular crystal as found above for the gas-phase molecules.

Calculations within the independent-particle approximation based on the PW91 electronic structure give a fair description of the first main absorption peak due to the partial cancellation of electronic self-energy and excitonic effects. They predict, however, a prominent absorption feature slightly below 5 eV which has not been detected experimentally. The calculations within the independent-particle approximation based on the HSE06 results, on the other hand, drastically overestimate the optical absorption energies. While the results obtained by solving the BSE yield the best agreement with experiment, the numerical expense involved in these calculations limits its application to small unit cells. Finally, we want to add a word of caution. The comparison between experiment and theory rests on the assumption that the experimental data represent a valid average of the ϵ_{xx}, ϵ_{yy}, and ϵ_{zz} components.

V. SUMMARY

In the present work the electronic structure and optical response of 2-aminopyrimidine-silver(I) based organic semiconductors and their parent molecules is analyzed on the basis of DFT as well as many-body perturbation theory calculations. The calculations predict quasiparticle gaps, i.e., differences between the ionization energies and electron affinities, of about seven eV for single FAP, OFAP, and NFAP molecules. The energies of the lowest optical excitations of the respective molecules are considerably lower. In fact, our result indicates a near cancellation of the electronic self-energy and exciton binding energies for the lowest excitations of 2-aminopyrimidines. The molecular crystals formed by silver(I) complex formation of these molecules differ in their electronic properties clearly from the parent molecules. The discrete molecular energy levels broaden into energy bands with a much (about one eV within DFT) reduced band gap. In addition, silver-related states appear close to the valence-band maximum. The latter states contribute only moderately to the optical transitions and the molecular fingerprints of FAP and OFAP are still clearly visible in the crystal optical response. This does not hold for NFAP, where the onset of the crystal optical absorption is strongly redshifted due to amino-group related transitions. While the optical absorption curves obtained within the IPA reproduce essentially the measured features, a quantitative agreement between experiment and measurement requires the consideration of many-body effects in the optical response calculations. In addition to electron-hole attraction effects that are instrumental for achieving satisfactory agreement between theory and experiment for many inorganic semiconductors, we additionally observe a very strong influence of local fields, i.e., the unscreened electron-hole exchange on the optical absorption of the organic semiconductors. Moreover, the resonant-nonresonant coupling terms in the excitonic Hamiltonian usually neglected in calculations for inorganic semiconductors are found to noticeably modify peak positions and oscillators strengths in the case of the molecular crystals studied here.

ACKNOWLEDGMENTS

We gratefully acknowledge financial support from the DFG and the Bielefeld University as well as supercomputer time provided by the HLRS Stuttgart and the Paderborn PC^2.

*riefer@mail.upb.de

[1] M. Rohlfing and S. G. Louie, Phys. Rev. Lett. **81**, 2312 (1998).
[2] S. Albrecht, L. Reining, R. DelSole, and G. Onida, Phys. Rev. Lett. **80**, 4510 (1998).
[3] M. Rohlfing, Int. J. Quantum Chem. **80**, 807 (2000).
[4] G. Onida, L. Reining, and A. Rubio, Rev. Mod. Phys. **74**, 601 (2002).
[5] P. H. Hahn, W. G. Schmidt, and F. Bechstedt, Phys. Rev. B **72**, 245425 (2005).
[6] W. G. Schmidt, Phys. Status Solidi B **242**, 2751 (2005).
[7] P. H. Hahn, W. G. Schmidt, K. Seino, M. Preuss, F. Bechstedt, and J. Bernholc, Phys. Rev. Lett. **94**, 037404 (2005).
[8] A. Hermann, W. G. Schmidt, and P. Schwerdtfeger, Phys. Rev. Lett. **100**, 207403 (2008).
[9] R. A. Mata, H. Stoll, and B. J. C. Cabral, J. Chem. Theory Comput. **5**, 1829 (2009).
[10] K. Hummer, C. Ambrosch-Draxl, G. Bussi, A. Ruini, M. Caldas, E. Molinari, R. Laskowski, and N. Christensen, Phys. Status Solidi B **242**, 1754 (2005).
[11] M. Grüning, A. Marini, and X. Gonze, Nano Lett. **9**, 2820 (2009).
[12] Y. Ma, M. Rohlfing, and C. Molteni, Phys. Rev. B **80**, 241405 (2009).
[13] C. Ambrosch-Draxl, K. Hummer, S. Sagmeister, and P. Puschnig, Chem. Phys. **325**, 3 (2006).
[14] K. Hummer, P. Puschnig, S. Sagmeister, and C. Ambrosch-Draxl, Mod. Phys. Lett. B **20**, 261 (2006).
[15] A. Ruini, M. J. Caldas, G. Bussi, and E. Molinari, Phys. Rev. Lett. **88**, 206403 (2002).
[16] I. Stoll, R. Brodbeck, B. Neumann, H.-G. Stammler, and J. Mattay, Cryst. Eng. Comm. **11**, 306 (2009).
[17] I. Stoll, R. Brockhinke, A. Brockhinke, M. Boettcher, T. Koop, H.-G. Stammler, B. Neumann, A. Niemeyer, A. Huetten, and J. Mattay, Chem. Mater. **22**, 4749 (2010).
[18] Crystallographic data CCDC 749826 - CCDC 749829 contain the supplementary crystallographic data for this paper. They can be obtained from the Cambridge Crystallographic Data Centre via [www.ccdc.cam.ac.uk].
[19] G. Kresse and J. Furthmüller, Comput. Mater. Sci. **6**, 15 (1996).
[20] J. P. Perdew, J. A. Chevary, S. H. Vosko, K. A. Jackson, M. R. Pederson, D. J. Singh, and C. Fiolhais, Phys. Rev. B **46**, 6671 (1992).
[21] P. E. Blöchl, Phys. Rev. B **50**, 17953 (1994).

[22]G. Kresse and D. Joubert, Phys. Rev. B **59**, 1758 (1999).
[23]M. A. Cazalilla, J. S. Dolado, A. Rubio, and P. M. Echenique, Phys. Rev. B **61**, 8033 (2000).
[24]A. Marini, R. Del Sole, and G. Onida, Phys. Rev. B **66**, 115101 (2002).
[25]R. M. Dreizler and E. K. U. Gross, *Density Functional Theory* (Springer-Verlag, Berlin, 1990).
[26]M. Preuss, W. G. Schmidt, K. Seino, J. Furthmüller, and F. Bechstedt, J. Comput. Chem. **25**, 112 (2004).
[27]T. Kowalczyk, S. R. Yost, and T. V. Voorhis, J. Chem. Phys. **134**, 054128 (2011).
[28]H.-C. Weissker, J. Furthmüller, and F. Bechstedt, Phys. Rev. B **69**, 115310 (2004).
[29]M. Shishkin and G. Kresse, Phys. Rev. B **74**, 035101 (2006).
[30]J. Heyd, G. E. Scuseria, and M. Ernzerhof, J. Chem. Phys. **118**, 8207 (2003).
[31]J. Heyd and G. E. Scuseria, J. Chem. Phys. **121**, 1187 (2004).
[32]J. Heyd, J. E. Peralta, G. E. Scuseria, and R. L. Martin, J. Chem. Phys. **123**, 174101 (2005).
[33]H. Ehrenreich and M. H. Cohen, Phys. Rev. **115**, 786 (1959).
[34]S. L. Adler, Phys. Rev. **126**, 413 (1962).
[35]N. Wiser, Phys. Rev. **129**, 62 (1963).
[36]M. Gajdos, K. Hummer, G. Kresse, J. Furthmüller, and F. Bechstedt, Phys. Rev. B **73**, 045112 (2006).
[37]V. Olevano and L. Reining, Phys. Rev. Lett. **86**, 5962 (2001).
[38]F. Bechstedt, R. Del Sole, G. Cappellini, and L. Reining, Solid State Commun. **84**, 765 (1992).
[39]A. Riefer, F. Fuchs, C. Rödl, A. Schleife, F. Bechstedt, and R. Goldhahn, Phys. Rev. B **84**, 075218 (2011).
[40]W. G. Schmidt, M. Albrecht, S. Wippermann, S. Blankenburg, E. Rauls, F. Fuchs, C. Rödl, J. Furthmüller, and A. Hermann, Phys. Rev. B **77**, 035106 (2008).
[41]F. Fuchs, C. Rödl, A. Schleife, and F. Bechstedt, Phys. Rev. B **78**, 085103 (2008).
[42]W. G. Schmidt, S. Glutsch, P. H. Hahn, and F. Bechstedt, Phys. Rev. B **67**, 085307 (2003).
[43]C. Ambrosch-Draxl, D. Nabok, P. Puschnig, and C. Meisenbichler, New J. Phys. **11**, 125010 (2009).
[44]A. Y. Golovacheva, A. N. Romanov, and V. B. Sulimov, J. Phys. Chem. A **109**, 3244 (2005).
[45]C. Freysoldt, P. Eggert, P. Rinke, A. Schindlmayr, and M. Scheffler, Phys. Rev. B **77**, 235428 (2008).
[46]J. B. Neaton, M. S. Hybertsen, and S. G. Louie, Phys. Rev. Lett. **97**, 216405 (2006).
[47]F. Fuchs, C. Rödl, A. Schleife, and F. Bechstedt, Phys. Rev. B **78**, 085103 (2008).
[48]The calculation of the Si electron-hole Hamiltonian is based on DFT-PBE (Ref. 49) wave functions and energies and a $12 \times 12 \times 12k$-point set.
[49]J. P. Perdew, K. Burke, and M. Ernzerhof, Phys. Rev. Lett. **77**, 3865 (1996).